

## Article

# Fabrication of a Gd<sub>2</sub>O<sub>3</sub>-Based Film to Shield from Space Radiation inside Aircraft and Its Effectiveness

Seon-Chil Kim <sup>1,2,\*</sup>  and Sung-Hwan Kim <sup>3</sup>

<sup>1</sup> Department of Biomedical Engineering, Keimyung University, 1095 Dalgubeol-daero, Daegu 42601, Republic of Korea

<sup>2</sup> Department of Medical Informatics, School of Medicine, Keimyung University, 1095 Dalgubeol-daero, Daegu 42601, Republic of Korea

<sup>3</sup> Department of Radiological Science, Cheongju University, Cheongju 28503, Republic of Korea; kimsh@cju.ac.kr

\* Correspondence: chil@kmu.ac.kr; Tel.: +82-10-4803-7773

**Abstract:** Aircraft are exposed to cosmic radiation depending on their flight altitude and latitude. Therefore, flight attendants are exposed to radiation for long periods. In this study, a 0.3 mm thick fabric was designed with which to manufacture crew clothes to shield them against external exposure to space radiation, and the shielding performance was analyzed based on empirical experiments in a real environment. Gadolinium oxide, which has a high neutron reaction cross-section, and tungsten, which is useful for gamma-ray shielding, were proposed as the main raw materials for the shielding fabric, and the shielding performance was evaluated using detectors on Arctic flight routes. Composite (KG-01) and single (KG-02) shielding materials were used. In the case of KG-01, the transmission dose rate was  $90.7 \pm 5.6\%$  compared with the unshielded case, showing an average space-radiation dose reduction of 9.3%. With KG-02, the transmission dose rate was  $103.1 \pm 2.0\%$  compared with the unshielded case, and the average dose rate increased by 3.1%; therefore, there was no shielding effect against space radiation. Considering the statistical error of the environmental radiation at aircraft flight altitudes, KG-01 had a shielding effect of at least 5%; however, KG-02 yielded no significant shielding effects.

**Keywords:** aviation shielding; radiation; gadolinium oxide; tungsten; radiation shielding



**Citation:** Kim, S.-C.; Kim, S.-H.

Fabrication of a Gd<sub>2</sub>O<sub>3</sub>-Based Film to Shield from Space Radiation inside Aircraft and Its Effectiveness.

*Aerospace* **2023**, *10*, 968. <https://doi.org/10.3390/aerospace10110968>

Academic Editor: Spiros Pantelakis

Received: 10 October 2023

Revised: 6 November 2023

Accepted: 14 November 2023

Published: 17 November 2023



**Copyright:** © 2023 by the authors. Licensee MDPI, Basel, Switzerland. This article is an open access article distributed under the terms and conditions of the Creative Commons Attribution (CC BY) license (<https://creativecommons.org/licenses/by/4.0/>).

## 1. Introduction

Depending on the flight altitude and latitude, aircraft are exposed to various radiation environments owing to the interaction between the spacecraft and the atmosphere. These environments expose crew members and passengers to radiation. Cosmic radiation can be divided into galactic cosmic rays (GCRs), solar energetic particles (SEPs) generated by solar flares or corona emissions, and radiation captured by the Earth's magnetic field [1,2]. GCRs are affected by solar activity and consist of protons, charged particles, alpha rays, and helium. SEPs have relatively lower energies than GCRs; however, they are composed of protons and electrons and are transmitted at higher fluxes compared with GCRs. Radiation doses change according to latitude, altitude, and time [3]. Figure 1 shows that various types of radiation are generated when space radiation interacts with the Earth's atmosphere. This radiation environment has variable characteristics during the flight of aircraft, depending on time and space [4]. Space radiation has a significant biological effect on the human body due to its high linear energy transfer (LET) [5]; during flight, the shielding effect of the atmosphere and the Earth's magnetic field is reduced and can thus have a significant biological effect on an aircraft's crew and passengers [6]. Unlike passengers, aircraft crew members work at high altitudes for long periods; therefore, they are more exposed to cosmic and secondary (scattered) radiation.

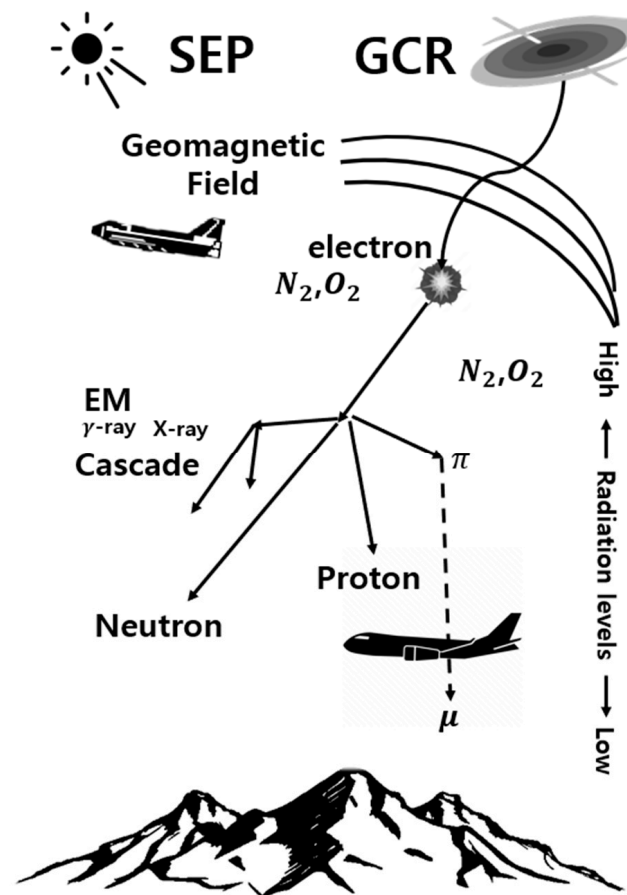


**Figure 1.** Radiation environment at commercial aircraft flight altitudes due to galactic cosmic rays (GCRs) and solar energetic particles (SEPs).

Figure 2a shows the type and dose of space radiation according to altitude. At altitudes in the range of 10–13 km, where international aircraft fly, the effects are primarily caused by secondary radiation generated from reactions with the Earth's atmosphere rather than the direct effects of cosmic radiation [7]. There are differences depending on latitude, altitude, and time. Figure 2a shows that for a total dose rate of approximately  $3.3 \mu\text{Sv/h}$  at an altitude of 10 km, the neutron, proton, electron, and other radiation dose rates are 1.8, 1.0, 0.2, and  $0.2 \mu\text{Sv/h}$ , respectively. The radiation dose contribution from neutrons and protons is 55% and 30%, respectively, accounting for 85% of the total radiation dose [8]. Figure 2b shows the dose of neutrons and charged particle radiation according to latitude; as latitude increases compared with that at the equator, the radiation dose increases by more than three times. A similar level of radiation environment is maintained for latitudes  $> 60^\circ$  [9]. The latitude dependence of radiation is caused by the distribution of the Earth's magnetic field.

Aircraft flying at high altitudes are exposed to considerably different radiation environments compared with the radiation environment on the ground, which can affect the crew, passengers, and electronic components of aircraft. Therefore, although complete shielding is difficult to achieve, research is required to reduce the damage caused by space radiation using flexible sheet-type shielding. Medical institutions and nuclear power plants are researching various shielding materials for X-rays and gamma rays; however, commercial products for space radiation shielding are still limited. Therefore, in this study, a sheet that can block neutrons and gamma rays was developed to produce a functional shielding fabric for flight attendants. Considering that neutrons contribute to more than 50% of space radiation, the material used to manufacture the sheet was mainly composed of gadolinium (Gd), which has a large neutron reaction cross-section, and tungsten (W), which can shield gamma rays. Because the sheet would be used as a shielding clothing material, it must

satisfy the low-weight, health, and flexibility requirements [10]. The shielding effect of the manufactured sheet was measured during an aircraft flight, and the results were compared with known data.

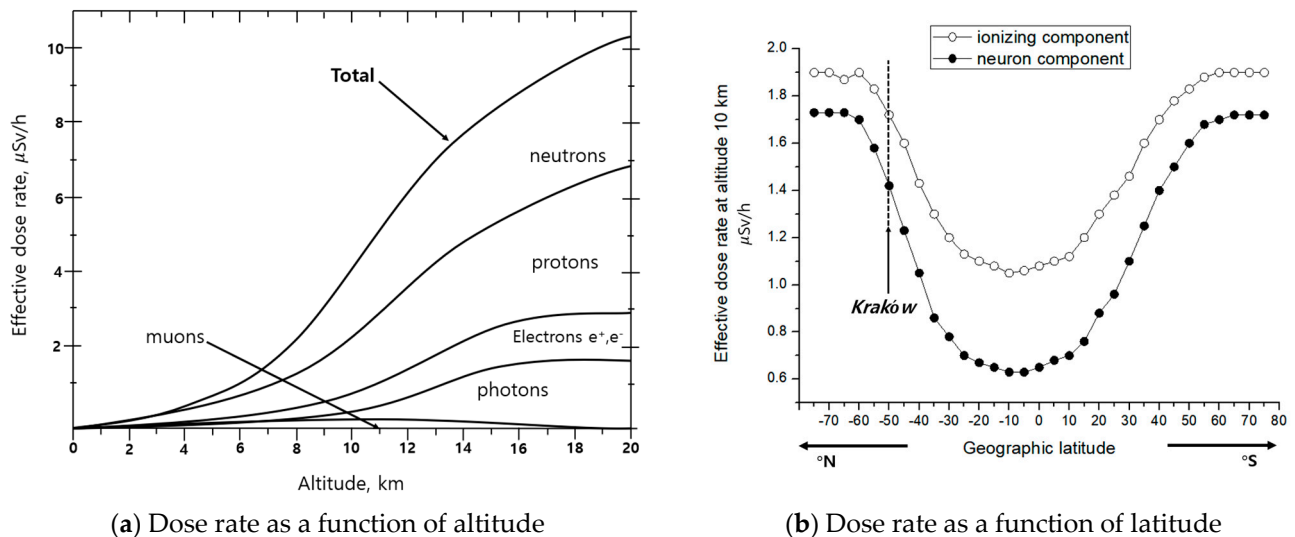


**Figure 2.** Types and dose rates of radiation according to altitude (a) and latitude (b).

## 2. Materials and Methods

### 2.1. Production of the Shielding Film

To protect against cosmic radiation, we fabricated a 0.3 mm thick functional shield. The shielding material was manufactured from powdered tungsten (W, 99.9%,  $<4\ \mu\text{m}$ , Nan-Gong XinDun Alloys Spraying Co., Ltd., Xingtai, China) and gadolinium oxide ( $\text{Gd}_2\text{O}_3$ ,  $<4\ \mu\text{m}$ , Duksan Pure Chemicals Co., Ltd., Ansan, Republic of Korea). The polymer used as the shielding material was dried polyurethane (PU, P-7195A, molecular weight (Mw) 100,000–150,000; Songwon, Republic of Korea). N-dimethylformamide (DMF, 99.5%, Daejung, Republic of Korea) was used as the solvent for polymer dissolution. Chloroform (95%, Duksan, Republic of Korea) was used as a poor solvent to control the volatilization rate. After the addition of the shielding material to the prepared spinning solution with 5.165 g of DMF and 2.785 g of chloroform, the mixture was dispersed for 1 min using an ultrasonic grinder; it was mixed at a speed of 600 revolutions per min (rpm) using a magnetic stirrer (Laboratory stirrer/hot plate, PC-420, Corning, Reynosa, Mexico). The polymer was completely dissolved and then spun. Two types of nanofibers were manufactured by mixing the PU spinning solution with the radiation-shielding material in a ratio of 7:3, followed by electrospinning, as shown in Figure 3. The first type, KG-01, was manufactured using 40 wt% gadolinium oxide and 30 wt% tungsten, and the second type, KG-02, was manufactured using 70 wt% gadolinium oxide alone. The injection speed of the spinning solution was adjusted to 0.6 mL/h using a syringe pump (KDS100, SD Scientific Inc., Holliston, MA, USA). A high-voltage power supply (CPS-60K02VIT, Chungpa EMT Co., Gyeonggi-do, Republic of Korea) was used. The radiation voltage was maintained at 10 kV after adjustment. The distance was adjusted to  $10 \pm 0.5\ \text{cm}$ , and the needle size was 22 gauge [11,12]. The external appearances of the manufactured shielding film membranes (KG-01 and KG-02) are shown in Figure 4. The degree of particle dispersion in the internal shielding material was measured using an optical microscope (field-emission scanning electron microscope (FESEM), S-4800, Hitachi, Tokyo, Japan) [13].

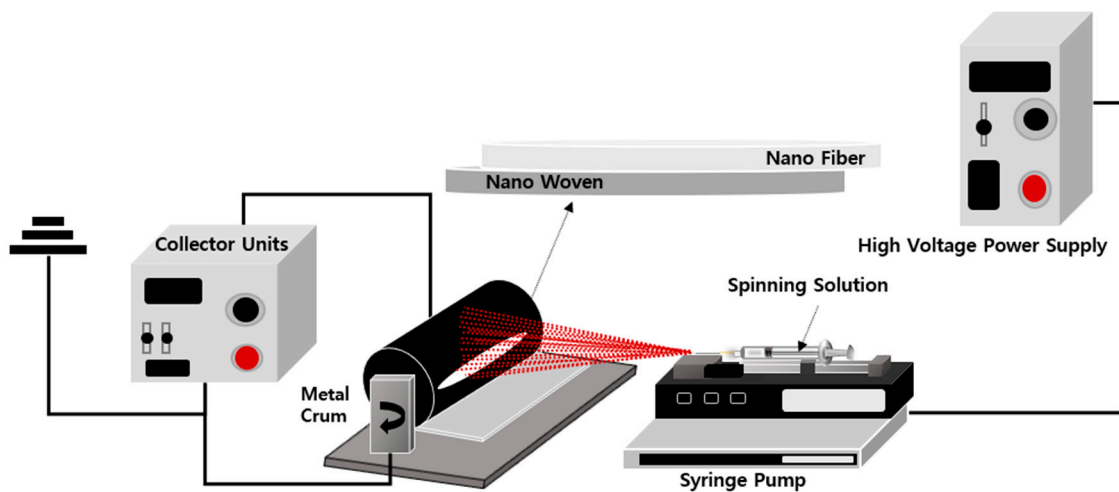


Figure 3. Schematic of the electrospinning process illustrated with images of the actual equipment.

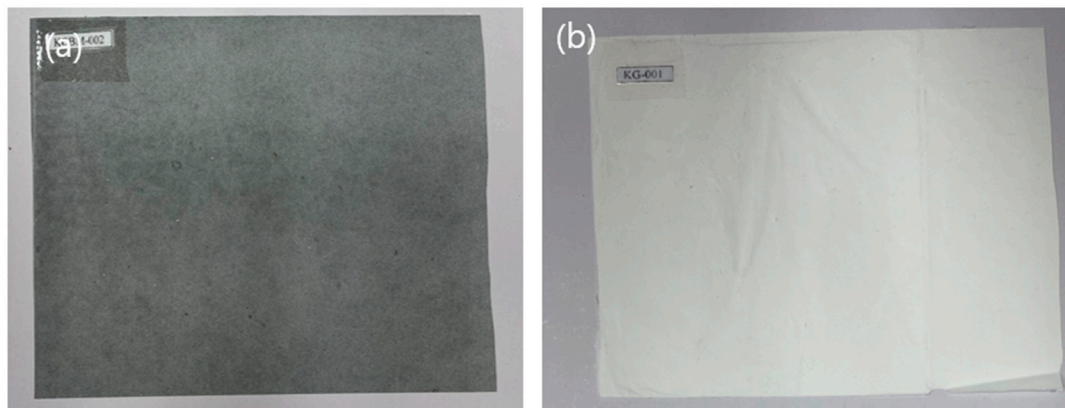


Figure 4. (a) Appearance of a 70% gadolinium oxide shielding film (KG-01), and (b) shielding film (KG-02) made by mixing 30% tungsten and 40% gadolinium oxide.

## 2.2. Dose Evaluation Algorithm

This study verified the radiation-shielding effect of the manufactured shielding films. Figure 5 shows the process of determining the equivalent dose from the measured pulse-height spectrum [14]. The Cosmic Ray Telescope for the Effects of Radiation (CRaTER), a space-radiation measuring instrument of the National Aeronautics and Space Administration, and the equivalent dose calculation algorithm were applied [15]. The pulse-height spectrum, measured using the *Si* sensor, was converted into a linear-energy spectrum based on energy correction. Because silicon has different density and atomic number from those of the human body, the measurement result for silicon must be adjusted accordingly to evaluate the dose applied to the human body. Benton et al. [16] showed that the LET values of several charged particle radiations measured on *Si* can be converted to LET values for the human body. Equation (1) converts  $LET_{Si}$ , determined through mathematical calculations for heavy ions with atomic numbers 1 to 54 with energies within 0.8 to 2000 MeV/amu, to the  $LET_{H_2O}$  [16]. The channels of the pulse-height spectrometer correspond to the energy of the measured radiation, and the energy  $E_i$  absorbed by each channel  $i$  can be summed over the total number of channels (1024) and divided by the mass of the sensor to determine the absorbed dose [17]. The equivalent dose in the human body was determined by applying the radiation weight factor ( $\omega_R$ ) from the International Commission on Radiological Protection Report 103 (ICRP 103) according to Equation (2) [18].  $\omega_R$  is a physical quantity introduced to compensate for differences in the biological effects of radiation on the human body depending on the LET of the radiation. At LETs below 10 keV/ $\mu\text{m}$ , there

is no increase in biological effects from radiation, thus  $\omega_R = 1$ . Above 10 keV/ $\mu\text{m}$ , the LET value determines  $\omega_R$ , as shown in Equation (2).

$$\log(LET_{H_2O}) = -0.2902 + 1.025 \log(LET_{Si}), \quad (1)$$

where LET is the linear energy transfer (keV/ $\mu\text{m}$ ), and

$$\omega_R = 1 \quad (LET \leq 10 \text{ keV}/\mu\text{m})$$

$$\omega_R = 0.32 \times LET - 2.2 \quad (10 \text{ keV}/\mu\text{m} < LET \leq 100 \text{ keV}/\mu\text{m}) \quad (2)$$

$$\omega_R = 300/LET \quad (100 \text{ keV}/\mu\text{m} < LET)$$

where  $\omega_R$  is the radiation weighting factor (ICRP 103).

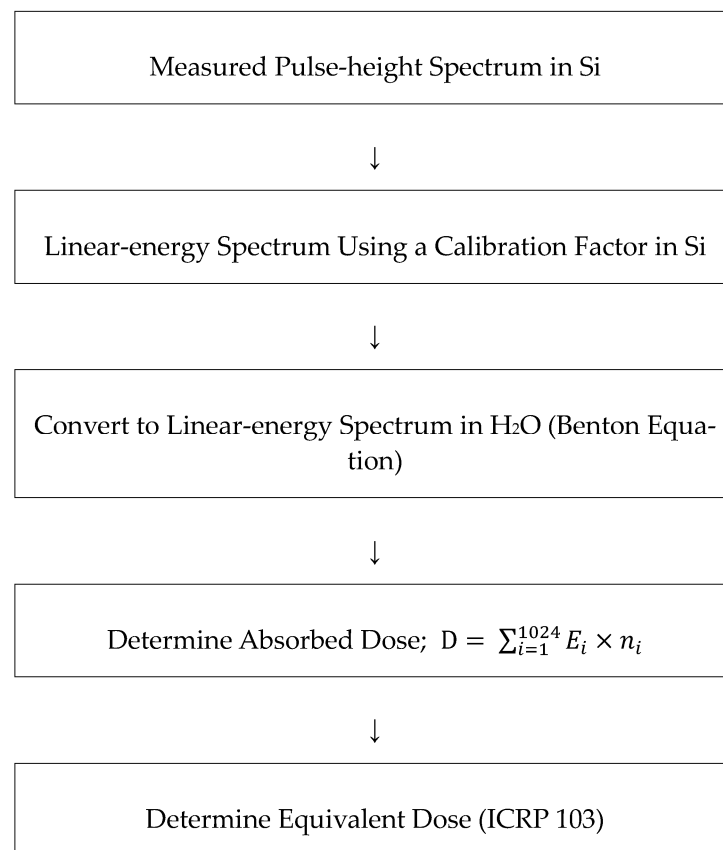


**Figure 5.** Space-radiation dose evaluation algorithm.

### 2.3. Space-Radiation Measuring Instrument

To verify the radiation protection effect of the shielding films produced in this study, a GDK-101 silicon sensor (GDK-101, FtLab Co., Ansan, Republic of Korea) was used, as shown in Figure 6a. This sensor consists of 10-pin photodiodes, operates in the counting mode, and has a measurable dose rate range of 0.01–200  $\mu\text{Sv/h}$  [19]. Considering the expected dose rate at the range of aircraft altitudes, it was judged to be suitable for dose assessments.

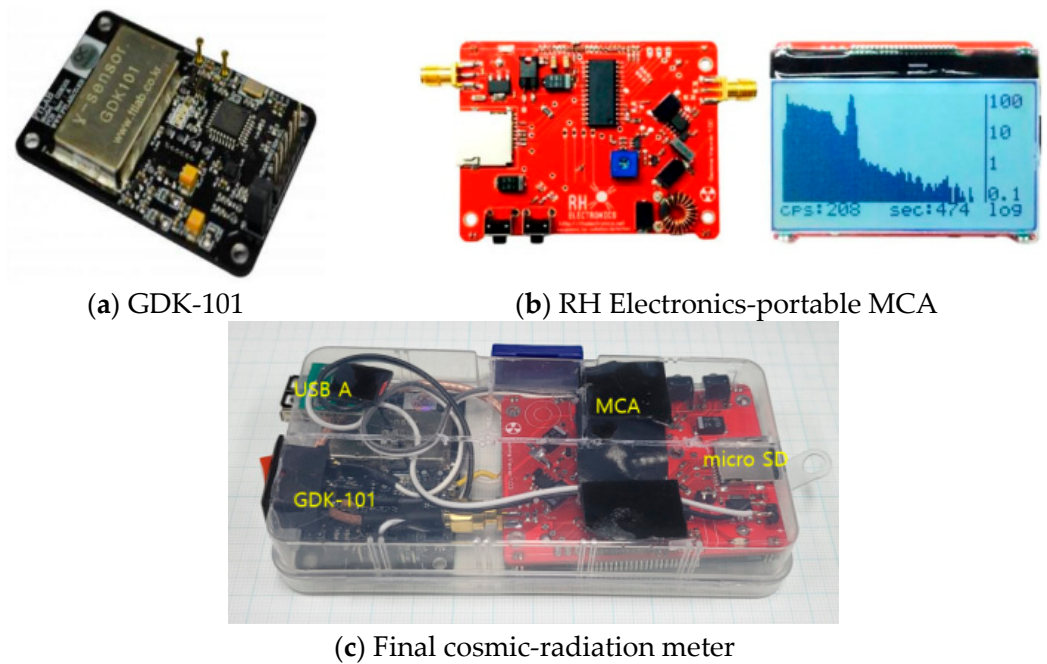


**Figure 6.** (a) Si-based radiation sensor, (b) multichannel pulse-height analyzer, and (c) space-radiation measuring instrument for evaluating space-radiation shielding characteristics at aircraft flight altitudes.

Although the GDK-101 sensor was designed to operate in the counting mode, the measurements confirmed that it outputs a signal proportional to the incident radiation energy, and the radiation energy spectrum was measured using this sensor. Figure 6b shows the general-purpose multichannel pulse-height analyzer from RH Electronics for measuring the energy spectrum. This consists of a programmable interrupt controller (PIC18) MCA module with 1024 channels and a 10-bit analog-to-digital converter.

The operating voltage was 5–12 V, and real-time spectrum confirmation was possible using a 128 × 64 liquid-crystal display. The measured data were saved on a microSD memory card, and the radiation dose measurement results were analyzed using a computer. Figure 6c shows the space-radiation detector manufactured using the GDK-101 sensor and RH Electronics MCA. A universal serial bus (USB)-A port was installed to use the USB power of the aircraft, and the measured spectral data were stored in a storage device installed in the microSD (secure digital) slot.

#### 2.4. Detector Calibration Test

Radiation detectors 1, 2, and 3 for the measured data value calibration experiment were obtained from a standard calibration institute for radiation detectors. Energy and dose calibrations were performed using Korasol's Cs-137 662 keV gamma-ray source at a dose rate of 10  $\mu\text{Sv/h}$ . In the case of GDK-101, the photoelectric peak of gamma rays could not be measured due to the small size of the Si sensor and the low atomic number; therefore, energy correction was performed by measuring the Compton edge, as shown in Equation (3). The Compton edge of the Cs-137 662 keV gamma ray was determined using Equation (3) to be 477 keV. Figure 7 shows the pulse-height spectrum measured for the Cs-137 662 keV gamma ray. The Compton edge channel was 77. From these results, the energy calibration factor was determined to be 6.2 keV/CH, and the dose-rate calibration factors for detectors 1, 2, and 3 were 0.598, 0.530, and 0.598 nSv/count, respectively.

$$E' = E_{\gamma} \left( 1 - \frac{1}{1 + \frac{2E_{\gamma}}{m_0c^2}} \right) \quad (3)$$

where

$E'$ : Compton edge energy (keV);

$E_\gamma$ : incident  $\gamma$  energy (keV);

$m_0$ : rest mass of electron (511 keV);

$c$ : velocity of light ( $3 \times 10^8$  m/s).

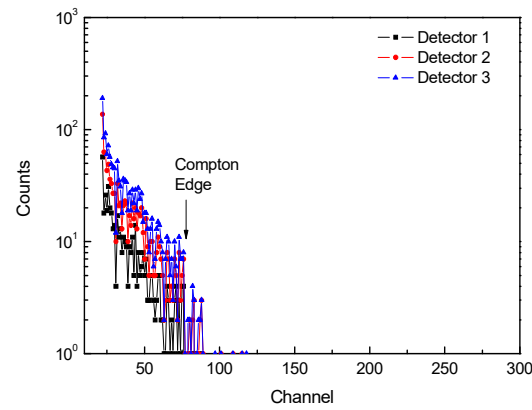


**Figure 7.** Energy calibration using a Cs-137 662 keV gamma-ray pulse-height spectrum and Compton edge.

### 3. Results

#### 3.1. Observation Results of the Internal Cross-Section of the Shielding Film

Figure 8 shows an internal cross-sectional view of the shielding films manufactured for protection from space radiation. The dispersion of the particle distribution of the shielding film mixed with tungsten and gadolinium oxide was better than that of the gadolinium oxide-only film. An even dispersion of particles imparts radiation protection, and this was the purpose of using nanofibers in the electrospinning model, where particles are evenly dispersed [20].

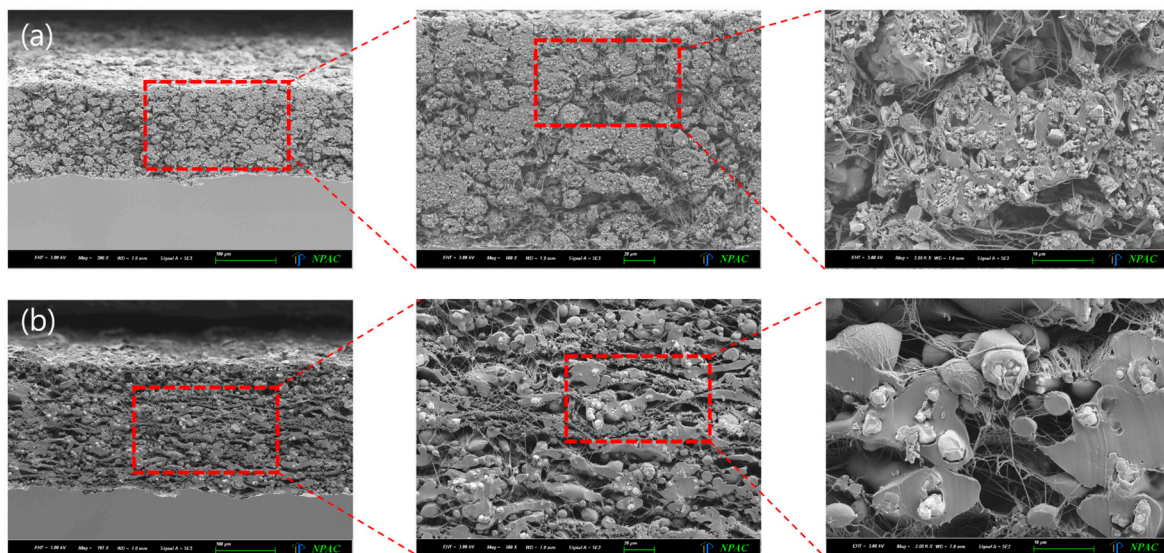
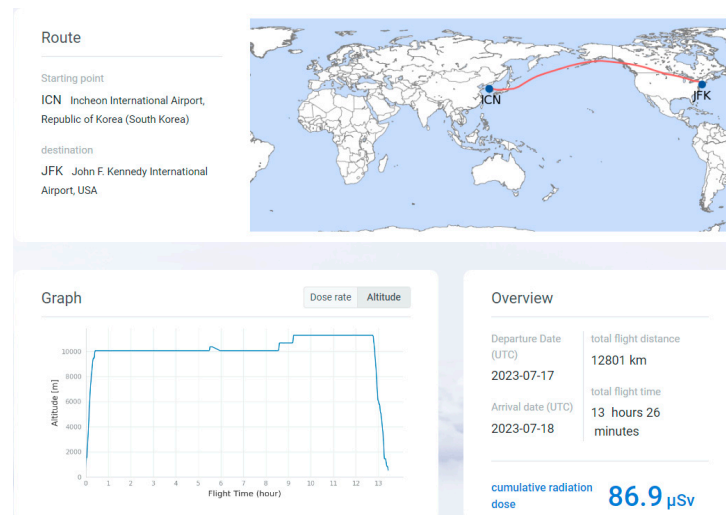


**Figure 8.** (a) Radiation shielding film made of 30% tungsten and 40% gadolinium oxide (KG-01), and (b) shielding film made of 70% gadolinium oxide (KGBM-002).

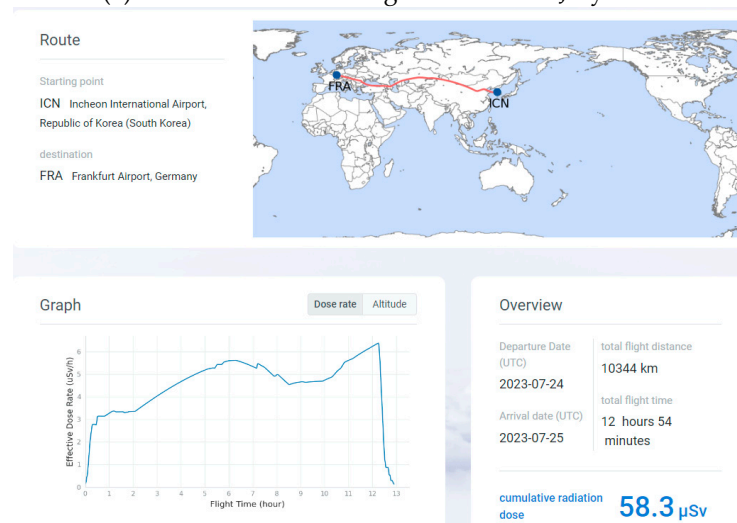
#### 3.2. Flight Test Route and Korean Radiation Exposure Assessment Model for Aviation Route Dose (KREAM): Estimated Dose Rate

Aviation shielding demonstration tests were conducted on the Incheon–New York, Incheon–Frankfurt, and Frankfurt–Incheon flights in July 2023. Detector 3 was used without

a shielding film, detector 1 was shielded with a KG-01 film, and detector 2 was shielded with a KG-02 film. The measured results were compared and analyzed at the end of the flights. The performance of the shielding film was evaluated using the ratio of values measured by detectors 2 and 1 and by detectors 3 and 1. The measurements were based on KREAM, jointly developed by the Korea Astronomy and Space Science Institute. Data from the National Meteorological Satellite Center of the Korea Meteorological Administration were used to compare and verify the space-radiation exposure dose by aircraft route and date [21]. Figure 9a shows the Incheon–New York flight route on 17 July 2023. The total flight time was 13 h and 26 min, the flight distance was 12,801 km, the total dose calculated using KREAM was 86.9  $\mu\text{Sv}$ , and the dose rate was 6.34  $\mu\text{Sv/h}$ . Figure 9b shows the Incheon–Frankfurt flight route on 24 July 2023. The total flight time was 12 h and 54 min, the flight distance was 10,334 km, the total dose calculated using KREAM was 58.3  $\mu\text{Sv}$ , and the dose rate was 4.52  $\mu\text{Sv/h}$ . Figure 9c shows the Incheon–Frankfurt flight route on 31 July 2023. The total flight time was 10 h and 52 min, the flight distance was 10,122 km, the total dose calculated using KREAM was 44.7  $\mu\text{Sv}$ , and the dose rate was 4.11  $\mu\text{Sv/h}$ . As the flight time and latitude increased, the amount of space radiation increased; the calculated dose rate during the Incheon–New York flight was the highest.

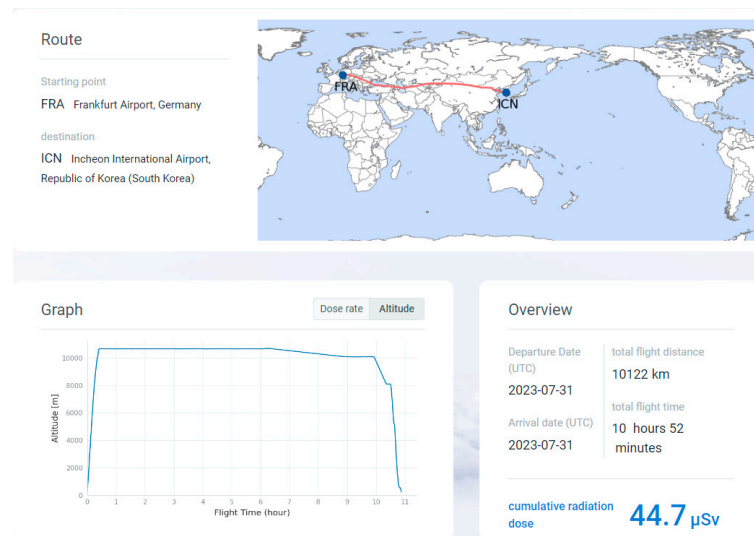


(a) Incheon–New York flight route on 17 July 2023



(b) Incheon–Frankfurt flight route on 24 July 2023

Figure 9. Cont.

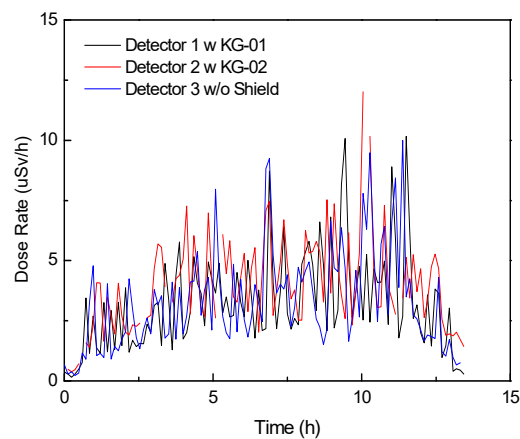


(c) Frankfurt–Incheon flight route on 31 July 2023

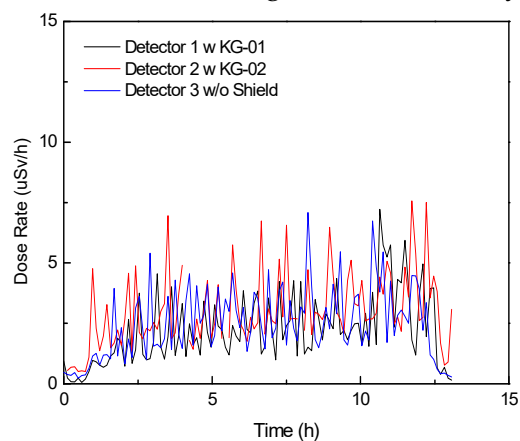
**Figure 9.** Air routes and dose rates were calculated using the Korean Radiation Exposure Assessment Model for Aviation Route Dose (KREAM).

### 3.3. Demonstration Test of the Space-Radiation Shielding Sheet using a Silicon Detector

Figure 10 shows the in-flight dose rates measured using the three detectors.

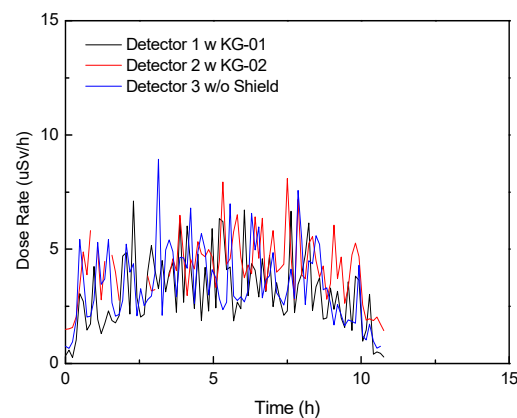


(a) Incheon–New York flight route on 17 July 2023



(b) Incheon–Frankfurt flight route on 24 July 2023

**Figure 10.** Cont.



(c) Frankfurt–Incheon flight route on 31 July 2023

**Figure 10.** Dose rate as a function of flight time according to the air route.

Table 1 lists the dose-rate measurement results for the three flights. Compared to the KREAM values, dose rate was 6.9% lower in the ICN–JFK section, 5.8% lower in the ICN–FRK section, and 9.7% lower in the FRK–ICN section. The Si sensor measurement value was found to be  $92.5 \pm 2.0\%$  of the KREAM value. The dose rate of space radiation varies depending on the flight section and time. In the case of neutrons, the dose rate may increase owing to secondary scattering rays caused by the shielding material.

**Table 1.** Measurements and Korean Radiation Exposure Assessment Model for Aviation Route Dose (KREAM) rates according to flight section.

Flight	Dose Rate ( $\mu\text{Sv/h}$ )			KREAM
	Detector 1 with KG-01	Detector 2 with KG-02	Detector 3 without ( <i>w/o</i> ) Shield	
2023.07 ICN–JFK	5.88	5.96	5.90	6.34
2023.07 ICN–FRK	3.84	4.37	4.26	4.52
2023.07 FRK–ICN	3.36	3.93	3.71	4.11

The space-radiation shielding effect of the manufactured shields was derived based on the results obtained when there was no shielding film, as listed in Table 2. The transmittance and shielding ratios were determined by comparing the average dose recorded using detectors 1 and 2 for the entire flight section (with shielding films) to that using detector 3 (without a shielding film). In the case of the KG-01 composite-material shielding, the transmission dose rate was  $90.7 \pm 5.6\%$ , compared with the unshielded dose-rate case, thus yielding an average space-radiation dose reduction of 9.3%. In the case of the KG-02 single-material shielding, the transmission dose rate was  $103.1 \pm 2.0\%$  compared with the unshielded case, and the average dose rate increased by 3.1%; therefore, there was no reduction in the space radiation dose. Considering the statistical uncertainties in environmental radiation levels at aircraft flight altitudes, KG-01 had a shielding effect of at least 5%, whereas KG-002 had no meaningful shielding effect. Therefore, a shielding film using tungsten and gadolinium oxide as composite materials was more effective than a single-material film made using gadolinium oxide.

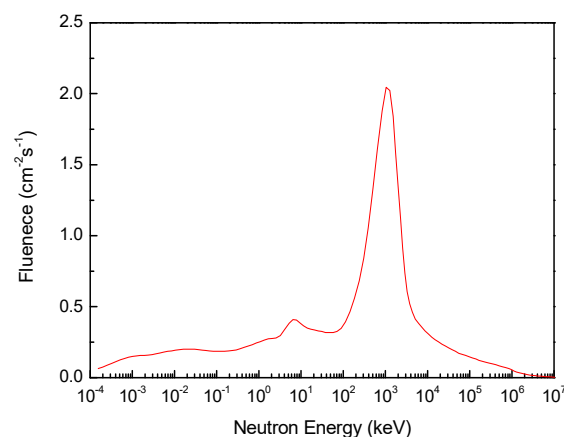
**Table 2.** Shielding ratio measurements on KG-01 and KG-02 air routes.

Flight	Ratio of the Dose Rate	
	$\frac{(\text{Det. 1 with KG-01})/(\text{Det. 3 w/o shield})}{(\%)}$	$\frac{(\text{Det. 2 with KG-02})/(\text{Det. 3 w/o shield})}{(\%)}$
2023.07 ICN-JFK	98.6	101.0
2023.07 ICN-FRK	87.9	102.5
2023.07 FRK-ICN	85.7	105.7
Trans. AVG (%)	90.7 ± 5.6	103.1 ± 2.0
Shielding (%)	+9.3%	−3.1%

#### 4. Discussion

Most particles that cause cosmic radiation effects at aviation altitudes (8–12 km) are high-energy space particles with MeV energies [22]. Owing to the Earth's magnetic field and atmosphere, only a small amount of cosmic radiation reaches inside aircraft. Protection from high-energy particles requires thick and dense shielding materials, which makes them heavy [23]. The space-radiation shielding effect can vary depending on the radiation absorption properties of the shield material for different subatomic particles, making it difficult to expect the same shielding effect against all particles [24]. In this study, two radiation shielding films, KG-02 (containing gadolinium oxide with a large neutron reaction cross-section) and KG-01 (containing gadolinium oxide and tungsten), were investigated to reduce the dose caused by space radiation at aircraft flight altitudes, and the dose-shielding effect was demonstrated through measurements during three flight routes [16]. Gadolinium oxide is a commonly used element in neutron detectors because of its large neutron reaction cross-section, which varies depending on the energy of neutrons; in the case of thermal neutrons, the neutron reaction cross-section of gadolinium is approximately  $4.9 \times 10^4$  b [25]. Tungsten has a thermal neutron reaction cross-section of 18.4 b, which is disadvantageous in shielding neutrons compared with gadolinium. However, tungsten has advantageous characteristics in shielding photons or charged particles owing to its high atomic number and density [26,27].

At aircraft flight altitudes, the proportion of the neutron dose from the ground is high (approximately 50%), and neutrons with an energy of approximately 1 MeV, which have the highest biological effect on the human body, are distributed in large quantities, as shown in Figure 11 [28,29].

**Figure 11.** Energy ratio of neutrons in cosmic radiation.

As shown in Figure 12, gadolinium has a high neutron reaction cross-section; therefore, it is effective in shielding low-energy neutrons. In the case of 1 MeV neutrons, the reaction cross-section is approximately 20 b, which is smaller than the reaction cross-section for thermal neutrons [30]. Therefore, if the shielding thickness is insufficient, the dose may

increase owing to secondary radiation generated by the reaction between fast neutrons and the shielding material, or neutrons whose energy is reduced because of the shielding material. The particle size of the shielding material affects the shielding effect [31,32].

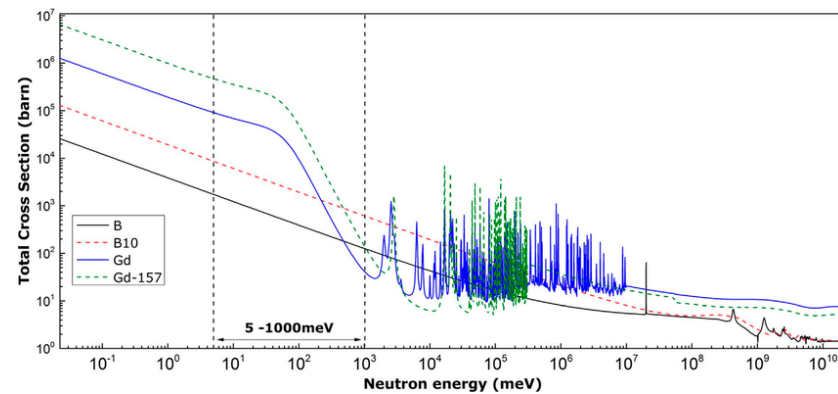


**Figure 12.** Comparison of cross-sectional areas for thermal neutrons of gadolinium (Gd).

In this empirical experiment, the dose-shielding effect of space-radiation shielding sheets was studied. Gadolinium oxide was found to be more effective in shielding cosmic radiation at aircraft flight altitudes when mixed with other materials than when used alone [33,34]. Shields using gadolinium oxide as a single material had no shielding effect. Shields made with a mixture of tungsten and gadolinium oxide had some shielding effect [35]. Within a certain margin of error, the quantitative dose of the single-material barrier increased. We speculate that this increase occurred because the incident high-energy particles were attenuated and scattered to the detector, resulting in the detection of higher doses [36]. Other studies reported measuring instruments detecting an increase in the background dose and scattered rays generated upon collision with the subject [37]. Use of a thin single material results in an unexpected cross effect and increased scattering through interactions [38]. This cross effect means that mutually symmetrical elements collide, thus increasing unwanted effects. This study had some limitations. The variability in environmental radiation was not considered for analysis. No analysis was conducted by varying the thickness of the manufactured shields. Although this study focused on fabrics for full-time protective clothing, their shielding potential was tested at low thickness and weight and without a high shielding rate. The shielding performance of a fabric varies depending on the type of radiation and particle interaction. It is difficult to expect the same shielding effect because protons, neutrons, and other particles can be produced in successive reactions. In this study, the shielding effect was investigated based on a 0.3 mm thick fabric, which is the limit of nanofiber production. Therefore, in order to produce shielding fabrics for flight crews, empirical evaluation based on the actual environmental conditions of flight routes is necessary. It is hoped that this study will stimulate related research [39].

## 5. Conclusions

To reduce the radiation dose to cabin crew members from space radiation at aircraft flight altitudes, a radiation shielding film containing gadolinium oxide with a large neutron reaction cross-sectional area and a shielding film containing gadolinium oxide and tungsten were manufactured. In the case of nanofiber-based shielding (thickness = 0.3 mm), the transmission dose rate was  $90.7 \pm 5.6\%$ , compared with the unshielded dose rate; this corresponded to an average space-radiation dose reduction effect of 9.3%.

**Author Contributions:** Conceptualization, S.-C.K.; methodology, S.-C.K.; validation, S.-H.K.; investigation, S.-C.K.; resources, S.-C.K.; data curation, S.-H.K.; writing—original draft preparation, S.-C.K.; writing—review and editing, S.-H.K.; supervision, S.-C.K.; project administration, S.-C.K.; funding acquisition, S.-C.K. All authors have read and agreed to the published version of the manuscript.

**Funding:** This study was supported by the Radiation Technology R&D program through the National Research Foundation of Korea funded by the Ministry of Science and ICT (2020M2C8A1056950). This research was also supported by the Basic Science Research Program through the National Research Foundation of Korea (NRF) funded by the Ministry of Education (2020R111A3070451).

**Data Availability Statement:** Data are contained within the article.

**Conflicts of Interest:** The author declares no conflict of interest.

## References

1. Yang, D.; Bayazitoglu, Y. Polymer composites as radiation shield against galactic cosmic rays. *J. Thermophys. Heat Transf.* **2020**, *34*, 457–464. [[CrossRef](#)]
2. Sato, T.; Kataoka, R.; Shiota, D.; Kubo, Y.; Ishii, M.; Yasuda, H.; Miyake, S.; Miyoshi, Y.; Ueno, H.; Nagamatsu, A. Nowcast and forecast of galactic cosmic ray (GCR) and solar energetic particle (SEP) fluxes in magnetosphere and ionosphere—extension of WASAVIES to Earth orbit. *J. Space Weather Space Clim.* **2019**, *9*, A10. [[CrossRef](#)]
3. Klein, E.M.; Sznajder, M.; Seefeldt, P. Proton Spectra for the Interplanetary Space Derived From Different Environmental Models. *Front. Space Technol.* **2022**, *3*, 933340. [[CrossRef](#)]
4. Tobiska, W.K.; Atwell, W.; Beck, P.; Benton, E.; Copeland, K.; Dyer, C.; Gersey, B.; Getley, I.; Hands, A.; Holland, M.; et al. Advances in atmospheric radiation measurements and modeling needed to improve air safety. *Space Weather* **2015**, *13*, 202–210. [[CrossRef](#)]
5. Jang, R.J. Literature review on cosmic radiation exposure to air craft cabin crew. *J. Radiol. Sci. Technol.* **2018**, *41*, 643–649. [[CrossRef](#)]
6. Sihver, L.; Kodaira, S.; Ambrožová, I.; Uchihori, Y.; Shurshakov, V. Radiation Environment Onboard Spacecraft at LEO and in Deep Space. In Proceedings of the 2016 IEEE Aerospace Conference, Big Sky, MT, USA, 1–9 March 2016. [[CrossRef](#)]
7. Bilski, P.; Olko, P.; Horwacik, T. Air-crew exposure to cosmic radiation on board of Polish passenger aircraft. *Nukleonika* **2004**, *49*, 77–83.
8. Dobynde, M.I.; Svertilov, S.I.; Panasyuk, M.I. Calculating the radiation dose rates created by cosmic rays in the Earth’s atmosphere. *Bull. Russ. Acad. Sci. Phys.* **2021**, *85*, 1302–1305. [[CrossRef](#)]
9. Mendes, M.M.; Darling, A.L.; Hart, K.H.; Morse, S.; Murphy, R.J.; Lanham-New, S.A. Impact of high latitude, urban living and ethnicity on 25-hydroxyvitamin D status: A need for multidisciplinary action? *J. Steroid Biochem. Mol. Biol.* **2019**, *188*, 95–102. [[CrossRef](#)]
10. Kim, S.C.; Son, J.S. Double-layered fiber for lightweight flexible clothing providing shielding from low-dose natural radiation. *Sci. Rep.* **2021**, *11*, 3676. [[CrossRef](#)]
11. Hou, J.; Park, C.; Jang, W.; Byun, H. Facile fabrication and characterization of aliphatic polyketone (PK) micro/nano fiber membranes via electrospinning and a post treatment process. *RSC Adv.* **2021**, *11*, 678–683. [[CrossRef](#)]
12. Yun, J.; Hou, J.; Jang, W.; Kim, S.Y.; Byun, H. Electrospun tungsten-polyurethane composite nanofiber mats for medical radiation-shielding applications. *ChemNanoMat* **2022**, *8*, e202100387. [[CrossRef](#)]
13. Liang, X.; Gao, G.; Wu, G. Statistical analysis on hollow and core-shell structured vanadium oxide microspheres as cathode materials for Lithium ion batteries. *Data Brief* **2018**, *18*, 719–722. [[CrossRef](#)]
14. Dietze, G.; Bartlett, D.T.; Cool, D.A.; Cucinotta, F.A.; Jia, X.; McAulay, I.R.; Pelliccioni, M.; Petrov, V.; Reitz, G.; Sato, T. ICRP PUBLICATION 123: Assessment of Radiation Exposure of Astronauts in Space. *Ann. ICRP* **2013**, *42*, 1–339. [[CrossRef](#)]
15. Schwadron, N.A.; Rahmanifard, F.; Wilson, J.; Jordan, A.P.; Spence, H.E.; Joyce, C.J.; Zeitlin, C. Update on the worsening particle radiation environment observed by CRaTER and implications for future human deep-space exploration. *Space Weather* **2018**, *16*, 289–303. [[CrossRef](#)]
16. Paek, S.W.; Balasubramanian, S.; Stupples, D. Composites Additive Manufacturing for Space Applications: A Review. *Materials* **2022**, *15*, 4709. [[CrossRef](#)]
17. Miroshnichenko, L.I. Radiation Conditions in Space. In *Radiation Hazard in Space. In Astrophysics and Space Science Library*; Springer: Dordrecht, The Netherlands, 2003; p. 297. [[CrossRef](#)]
18. Semwal, M.K. International Commission on Radiological Protection Report 152(2022): Radiation detriment calculation methodology. *J. Med. Phys.* **2023**, *48*, 98–99. [[CrossRef](#)]
19. Hess, W.N.; Patterson, H.W.; Wallace, R.; Chupp, E.L. Cosmic-ray neutron energy spectrum. *Phys. Rev.* **1959**, *116*, 445–457. [[CrossRef](#)]
20. Khong, J.C.; Daisenberger, D.; Burca, G.; Kockelmann, W.; Tremsin, A.S.; Mi, J. Design and characterization of metallic glassy alloys of high neutron shielding capability. *Sci. Rep.* **2016**, *6*, 36998. [[CrossRef](#)]
21. Hwang, J.A.; Kwak, J.Y.; Jo, G.B.; Nam, U.W. Validation of KREAM based on in-situ measurements of aviation radiation in commercial flights. *J. Astron. Space Sci.* **2020**, *37*, 229–236. [[CrossRef](#)]
22. Osunwusi, A.O. Occupational radiation exposures in aviation: Air traffic safety systems considerations. *Int. J. Aviat. Aeronaut. Aerosp.* **2020**, *7*, 6. [[CrossRef](#)]
23. Spence, H.E.; Case, A.W.; Golightly, M.J.; Heine, T.; Larsen, B.A.; Blake, J.B.; Caranza, P.; Crain, W.R.; George, J.; Lalic, M.; et al. CRaTER: The cosmic ray telescope for the effects of radiation experiment on the lunar reconnaissance orbiter mission. *Space Sci. Rev.* **2010**, *150*, 243–284. [[CrossRef](#)]

24. Loffredo, F.; Vardaci, E.; Pugliese, M.; Serra, M.; Quarto, M. Dosimetry in Space: The shielding effectiveness for the radioprotection of astronauts against 1 GeV protons. *IL Nuovo Cimento C* **2020**, *43*, 133. [[CrossRef](#)]
25. Kobayashi, M.; Ieiri, M.; Kondo, K.; Miura, T.; Noumi, H.; Numajiri, M.; Oki, Y.; Suzuki, T.; Takasaki, M.; Tanaka, K.; et al. Radiation hardness of cerium-doped gadolinium silicate Gd<sub>2</sub>SiO<sub>5</sub>:Ce against high energy protons, fast and thermal neutrons. *Nucl. Instrum. Methods Phys. Res. Sect. A Accel. Spectrometers Detect. Assoc. Equip.* **1993**, *330*, 115–120. [[CrossRef](#)]
26. Cheewasukhanont, W.; Limkitjaroenporn, P.; Sayyed, M.I.; Kothan, S.; Kim, H.J.; Kaewkhao, J. High density of tungsten gadolinium borate glasses for radiation shielding material: Effect of WO<sub>3</sub> concentration. *Radiat. Phys. Chem.* **2022**, *192*, 109926. [[CrossRef](#)]
27. Azman, M.N.; Abualroos, N.J.; Yaacob, K.A.; Zainon, R. Feasibility of nanomaterial tungsten carbide as lead-free nanomaterial-based radiation shielding. *Radiat. Phys. Chem.* **2023**, *202*, 110492. [[CrossRef](#)]
28. Sato, T. Recent progress in space weather research for cosmic radiation dosimetry. *Ann. ICRP* **2020**, *49* (Suppl. S1), 185–192. [[CrossRef](#)]
29. Yasuda, H.; Kurita, N.; Yajima, K. Verification of estimated cosmic neutron intensities using a portable neutron monitoring system in Antarctica. *Appl. Sci.* **2023**, *13*, 3297. [[CrossRef](#)]
30. Dumazert, J.; Coulon, R.; Lecomte, Q.; Bertrand, G.H.V.; Hamel, M. Gadolinium for neutron detection in current nuclear instrumentation research: A review. *Nucl. Instrum. Methods Phys. Res. Sect. A Accel. Spectrometers Detect. Assoc. Equip.* **2018**, *882*, 53–68. [[CrossRef](#)]
31. Chang, Q.; Guo, S.; Zhang, X. Radiation shielding polymer composites: Ray-interaction mechanism, structural design, manufacture and biomedical applications. *Mater. Des.* **2023**, *233*, 112253. [[CrossRef](#)]
32. Kim, S.C. Analysis of shielding performance of radiation-shielding materials according to particle size and clustering effects. *Appl. Sci.* **2021**, *11*, 4010. [[CrossRef](#)]
33. Shreef, A.M.; Abdulzahara, N.A. Manufacture of shielding for attenuation ionization ray by the preparation of nano gadolinium oxide with PMMA. *NeuroQuantology* **2021**, *19*, 66. [[CrossRef](#)]
34. Zhang, P.; Jia, C.; Li, J.; Wang, W. Shielding composites for neutron and gamma-radiation with Gd<sub>2</sub>O<sub>3</sub>@W core-shell structured particles. *Mater. Lett.* **2020**, *276*, 128082. [[CrossRef](#)]
35. Hannachi, E.; Sayyed, M.I.; Slimani, Y.; Elsafi, M. Structural, optical and radiation shielding peculiarities of strontium titanate ceramics mixed with tungsten nanowires: An experimental study. *Opt. Mater.* **2023**, *135*, 113317. [[CrossRef](#)]
36. Obaid, S.S.; Sayyed, M.I.; Gaikwad, D.K.; Pawar, P.P. Attenuation coefficients and exposure buildup factor of some rocks for gamma ray shielding applications. *Radiat. Phys. Chem.* **2018**, *148*, 86–94. [[CrossRef](#)]
37. Poitrasson-Rivière, A.; Hamel, M.C.; Polack, J.K.; Flaska, M.; Clarke, S.D.; Pozzi, S.A. Dual-particle imaging system based on simultaneous detection of photon and neutron collision events. *Nucl. Instrum. Methods Phys. Res. Sect. A Accel. Spectrometers Detect. Assoc. Equip.* **2014**, *760*, 40–45. [[CrossRef](#)]
38. Cole, J.M.; Behm, K.T.; Gerstmayr, E.; Blackburn, T.G.; Wood, J.C.; Baird, C.D.; Duff, M.J.; Harvey, C.; Ilderton, A.; Joglekar, A.S.; et al. Experimental evidence of radiation reaction in the collision of a high-intensity laser pulse with a laser-wakefield accelerated electron beam. *Phys. Rev. X* **2018**, *8*, 011020. [[CrossRef](#)]
39. Blachowicz, T.; Ehrmann, A. Shielding of cosmic radiation by fibrous materials. *Fibers* **2021**, *9*, 60. [[CrossRef](#)]

**Disclaimer/Publisher's Note:** The statements, opinions and data contained in all publications are solely those of the individual author(s) and contributor(s) and not of MDPI and/or the editor(s). MDPI and/or the editor(s) disclaim responsibility for any injury to people or property resulting from any ideas, methods, instructions or products referred to in the content.